



## **Novel Dual-Band SIW-To-Metal Waveguide Transition with Integrated Filtering for Diplexing 77GHz and 130GHz Frequency Bands**

Downloaded from: <https://research.chalmers.se>, 2026-04-19 08:54 UTC

Citation for the original published paper (version of record):

Van Hastenberg, K., Ivashina, M., Smolders, A. et al (2025). Novel Dual-Band SIW-To-Metal Waveguide Transition with Integrated Filtering for Diplexing 77GHz and 130GHz Frequency Bands. Eucap 2025 19th European Conference on Antennas and Propagation. <http://dx.doi.org/10.23919/EuCAP63536.2025.10999541>

N.B. When citing this work, cite the original published paper.

# Novel Dual-Band SIW-To-Metal Waveguide Transition with Integrated Filtering for Diplexing 77GHz and 130GHz Frequency Bands

Kevin A.P. van Hastenberg\*, Marianna V. Ivashina<sup>†</sup>, A. Bart Smolders\*, and Artem R. Vilenskiy<sup>†</sup>

\*Eindhoven University of Technology, Electromagnetics Group, Eindhoven, The Netherlands

<sup>†</sup>Chalmers University of Technology, Antenna Group, Göteborg, Sweden

Corresponding author: k.a.p.v.hastenberg@tue.nl

**Abstract**—This paper presents a novel dual-band transition from a substrate-integrated waveguide (SIW) to two air-filled waveguides (WGs) operating at 77 GHz and 130 GHz, targeting applications such as automotive radar systems. The proposed structure incorporates a diplexing mechanism to effectively combine/separate the two frequency bands, allowing them to share a common WG environment while keeping their signals distinct. The diplexer consists of a filter in the 77 GHz WG, blocking the 130 GHz signals, and a below cut-off SIW and WG in the 130 GHz signal path, providing inherent filtering for the 77 GHz signal. This inherent filtering helps minimize the size compared to that of classical filter-type diplexers. The reduced size comes at the cost of a lower isolation between the two WG outputs. The proposed structure overcomes the limitations of existing single-band transition designs by reducing the insertion loss to below 1 dB in each band, achieving a wide bandwidth, and ensuring good matching performance. Furthermore, the predicted isolation is at least 15 dB at 77 GHz and at least 40 dB at 130 GHz, and an insertion loss of 0.6 dB at 77 GHz and 0.4 dB at 130 GHz is achieved. The insertion loss is increased by the inclusion of surface roughness in the metal mainly at 77 GHz due to the presence of the filter.

**Index Terms**—Dual-frequency, 77GHz, 130GHz, transition, waveguide filter, diplexer, SIW

## I. INTRODUCTION

As the carrier frequency of modern communication and sensing systems continues to increase, so do the losses associated with transferring these signals from an integrated circuit (IC) to the antennas. An example of increased losses can be seen in solder ball transitions [1], which are present in many millimeter-wave (mmWave) products and carry the RF signals from an IC to a PCB carrier. Besides the increased transition losses, printed transmission line losses increase with frequency as well and are restricted in using vertical transitions due to additional losses created by much-used via structures. A possible solution to both problems is to launch the signals from an IC directly into a waveguide (WG) structure, reducing the transition loss and routing losses while maintaining a high degree of freedom. In this way, an IC could, for instance, be connected directly to WG antennas in a low-loss manner.

In general, two types of transition between an IC and a WG can be distinguished: a transverse (inline) and a vertical (orthogonal) transition. Examples of transverse transitions are shown in [2]–[5] and examples of vertical transitions are

shown in [6]–[8]. As is evident in these prototypes, there is a great variety in complexity for these designs. Preferably, such a transition would consist of accessible cost-effective solutions, a structure that is low-sensitive to positioning errors and allows for a lot of freedom in routing the metal WGs.

One of the applications at mmWave frequencies that will see increased activity in the coming years is automotive radar, caused by the goal to have self-driving cars, which require more and more accurate data of their surroundings. From an IC perspective, it might be interesting to combine hardware between the 77 GHz and 130 GHz automotive radar bands to minimize the chip area and reduce costs. Furthermore, aggregating data at two different frequencies on-chip might lead to more efficient detection and mapping. However, from an antenna perspective, there are some constraints when creating an extreme wideband antenna array. The largest antenna element size, dictated by the lowest frequency, typically does not fit in the allowed array grid spacing of half-wavelength, dictated by the highest frequency to avoid grating lobes. A solution is to split the RF output of this IC into two different antenna arrays, allowing both arrays to be optimized without compromise. This routing flexibility would be possible in metal WGs because of their low loss per unit length. Nevertheless, this solution requires a diplexer at the IC output to effectively decouple the two distinct antenna arrays.

To tackle the aforementioned problems, this paper proposes using a low-loss dual-band vertical transition from a substrate-integrated waveguide (SIW) to two air-filled WGs operating at 77 GHz and 130 GHz, having an integrated diplexing functionality. Such an SIW can either be incorporated directly on-wafer or be implemented on an intermediate planar structure. In this study, the vertical transition architecture is selected, allowing more design flexibility for dual-band operation and lower positioning sensitivity compared to the inline architecture. Moreover, assembly of the vertical transition is simpler due to many horizontal transitions requiring a split-block assembly. By addressing the shortcomings of aforementioned designs and by expanding the concept to a dual-band implementation a novel transition is proposed.

The paper is structured as follows; the design is discussed in Section II after which simulation results are shared in Section III. Finally, a discussion and conclusion are presented

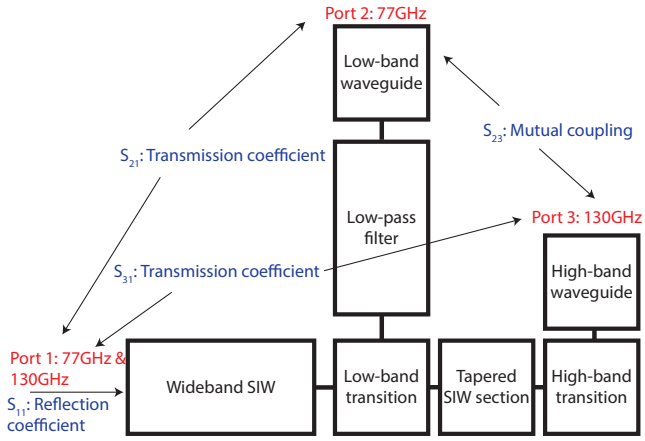


Fig. 1. Block diagram of the proposed transition highlighting the ports and important metrics.

in Section IV.

## II. DESIGN

In the remainder of this paper Port 1 refers to the common 77 GHz and 130 GHz SIW port on the PCB, whereas Port 2 and Port 3 correspond with the 77 GHz and 130 GHz ports of the air-filled WG, respectively, as seen in the block diagram in Fig. 1.

The prototype consists of a metal part that includes the low-band and high-band WG blocks and the low-pass filter (LPF) block, and a PCB part which includes the SIW blocks and both transition blocks. Instead of embedding a classical 2-filter diplexer inside the metal block, it was decided to use the coupling mechanism from the SIW to metal WGs as part of the filtering capabilities of the diplexer. This reduces the size of the design and also eases the requirements on the coupling transition, as these only need to be optimized for a single frequency range. For the frequency output at 130 GHz, a tapered SIW is used to filter out the 77 GHz band, for which the tapered section's output SIW is below the TE<sub>10</sub> mode cut-off. So, the two transitions together with the LPF act as the diplexer in this design. The important metrics to optimize for this transition are the reflection coefficient,  $S_{11}$ , the transmission coefficients,  $S_{21}$  and  $S_{31}$ , and the mutual coupling,  $S_{23}$ . This last parameter is specifically relevant for dual-band transition. Some relevant sources are summarized in Table I together with the type of transition. The type includes whether it is a transverse or vertical transition.

The proposed design is shown in Fig. 2 where the tapered section can be seen in the green dashed area. In this graph, the two coupling slots are also shown which are used to couple to the two separate WGs in the metal block.

For the low-band WG at Port 2, the transmission of the 130 GHz signal is not blocked. Therefore, a four-stage LPF is implemented in the the same WG environment to filter out the high-band components and provide their high-efficiency transmission towards Port 3. The LPF is implemented in the E-plane by using capacitive irises and cavities. The LPF

TABLE I  
IMPORTANT METRICS FROM MEASURED DESIGNS IN LITERATURE. BW: BANDWIDTH, IL: INSERTION LOSS, RL: RETURN LOSS

Ref.	BW (GHz)	IL (dB) (single)	RL (dB)	Type
[2]	85 – 105(21%)	0.5 – 0.75	$\geq 10$	Transverse. SIW to ridge WG (gap-wave)
[3]	40 – 60(40%)	$\leq 2.5^1$	$\geq 8$	Transverse. Probe-coupling
[4]	80 – 114	$\leq 0.4$	$\geq 13$	Transverse. Cavity with probe (gap-wave)
[5]	75 – 110	$\leq 0.8$	$\geq 10$	Transverse. SIW to ridge WG
[6]	85.7 – 104.5	1.7 – 2.3	$\geq 10$	Vertical. Slot-coupled rectangular patch
[7]	24.5 – 37.8	$< 0.3$	$\geq 10$	Vertical. Aperture to stepped ridge WG
[8]	54 – 67	$\leq 0.58$	$\geq 11$	Vertical. Slot to slot-coupled rectangular patch

<sup>1</sup> Includes measurement adapter losses

provides a highly suppressed stopband in between 120 GHz to 140 GHz. During synthesis, the LPF feature size was restricted to 100  $\mu\text{m}$  to make sure manufacturability is guaranteed.

The SIW is realized by simply creating rows of vias with an electrically small spacing in between two ground planes. A 0.508 mm thick RO4003C substrate is used for the PCB substrate. It has a relative permittivity of  $\epsilon_r = 3.38$  and a loss tangent  $\tan \delta = 0.0027$ . The vias are spaced 300  $\mu\text{m}$  apart with an outer via diameter of 200  $\mu\text{m}$ . An additional row of vias is placed along the internal row to make sure leakage is minimized in the high-band.

As seen in Fig. 2, the WGs are routed in two different directions. This was deliberately chosen so that testing is easier when connecting external WG test ports. This was also the reason for introducing the bend in the Port 2 WG section allowing for back-to-back structure testing.

The impedance-matching optimization resulted in the low-frequency coupling slot being electrically narrow, providing the transition operation in the aperture-coupling manner. At the same time, the electrically wide high-frequency coupling slot provides a transition operation similar to the 90-degree E-plane WG bend. The extension of the SIW after the second slot is 0.66 mm, which is approximately  $\frac{\lambda}{2}$  at 130 GHz, is used to provide extra space required to accommodate the coupling slot while preserving impedance matching. The air-filled WGs themselves are also thinner, compared to the rectangular EIA WG standards, to match their characteristic impedance to the SIW. The characteristic impedance of WGs can be evaluated with [9], [10]

$$Z = \frac{Z^\infty}{\sqrt{1 - (f_c/f)^2}}, \quad (1)$$

with  $Z^\infty$  the high-frequency impedance asymptotics and  $f_c$  the

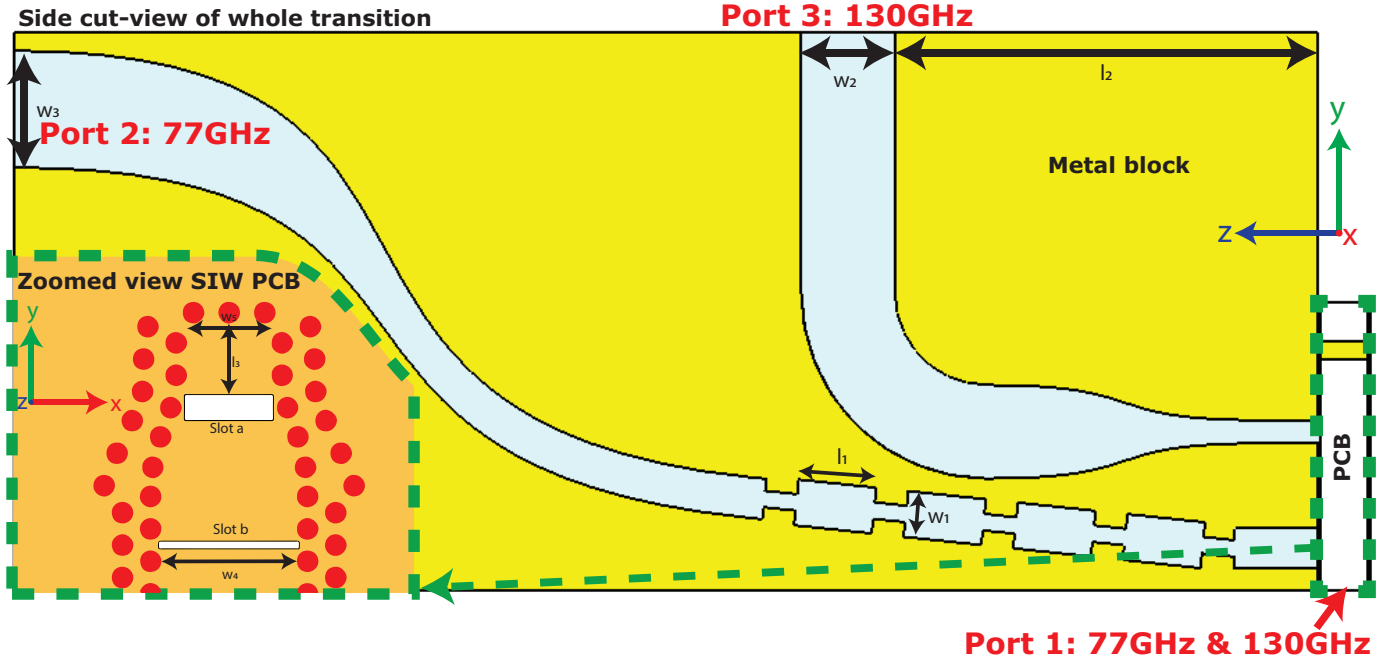


Fig. 2. Implementation of block diagram in Fig. 1 showing the metal block and the SIW on PCB. A zoomed view of the SIW on PCB is given in the green box.  $l_1 = 0.85$  mm,  $l_2 = 4.60$  mm,  $l_3 = 0.66$  mm,  $w_1 = 0.85$  mm,  $w_2 = 1.02$  mm,  $w_3 = 1.27$  mm,  $w_4 = 1.25$  mm,  $w_5 = 0.78$  mm

mode cut-off frequency described as follows:

$$Z^\infty = \frac{\pi^2}{8} \frac{120\pi}{\sqrt{\epsilon_r}} \frac{H}{W'}, \quad f_c = \frac{c_0}{2W'\sqrt{\epsilon_r}}, \quad (2)$$

where  $\epsilon_r$  is the relative permittivity,  $c_0$  is the speed of light in vacuum,  $H$  is the height of the WG and  $W'$  the effective width of the WG. This effective width is the physical width for the air-filled WG and is described by  $W'_{SIW} = W_{SIW} - \frac{D^2}{0.95P}$  for the SIW, where  $D$  and  $P$  are the via diameter and period, respectively.

The resulting heights of the air-filled WGs after some manual optimization are 0.44 mm and 0.25 mm for 77 GHz and 130 GHz, respectively. Each of the WG channels tapers to standard WR-12 for Port 2 and WR-8 for Port 3 after the transition. The resulting SIW widths for a fixed height of 0.508 mm are 1.25 mm and 0.78 mm for 77 GHz and 130 GHz, respectively.

### III. RESULTS

All simulations were performed in CST studio suite with the frequency domain solver. The first component which was simulated was the LPF. The response of the LPF can be seen in Fig. 3. All of the metal blocks were designed from aluminum. As it is yet unknown in which process the metal block is going to be manufactured, a surface roughness of  $R_a = 4$   $\mu\text{m}$  was used for comparison with a simulation neglecting surface roughness. This surface roughness would be achievable with a selective laser melting (SLM) 3D printer after using post-processing on the part [11]. The advantage of 3D printing this part would be the fact that no split-block assembly is needed as this will inevitably lead to leakage

between the two halves at 130 GHz. The results in Fig. 3 show that the surface roughness increases the insertion loss by approximately 0.5 dB at 77 GHz. There is a wide impedance match in the low-band and a high isolation of at least 30 dB in the high-band.

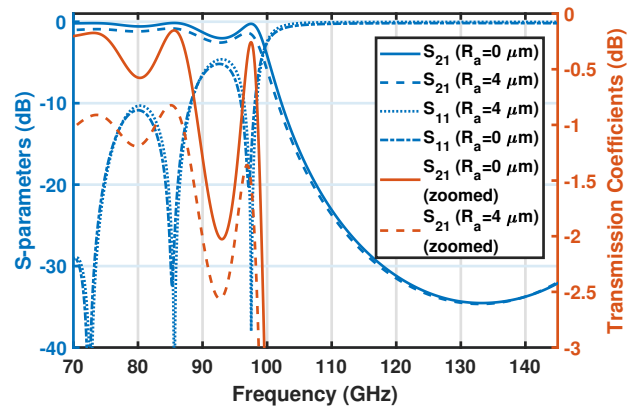


Fig. 3. S-parameters of the LPF, with and without surface roughness, including a zoomed plot of the transmission coefficient on the right axes.

In Fig. 4 the S-parameters for the single-ended transition, shown in Fig. 2, are plotted. The reflection coefficient around 77 GHz and 130 GHz is below  $-15$  dB with the insertion loss being around 0.6 dB for the low-band and around 0.4 dB for the high-band. The  $-10$ -dB BW is 4.5 GHz and 29 GHz for the 77 GHz and 130 GHz bands, respectively. Note that these results are without including surface roughness.

The isolation between the different ports can be seen in

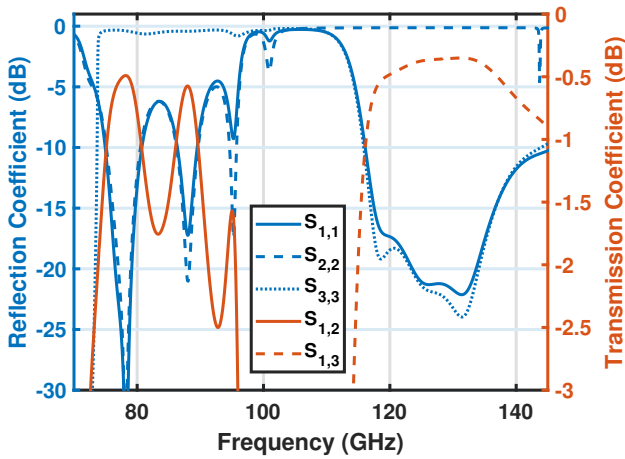


Fig. 4. S-parameters of the single-ended transition, without surface roughness.

Fig. 5. As is evident from this plot, the transmission coefficient  $S_{31}$  is below  $-15$  dB at 77 GHz. This isolation is mainly caused by the tapered SIW, and a WG size at Port 3 which is below cut-off for 77 GHz. If stricter isolation requirements are necessary, an additional filter can also be implemented in the Port 3 WG as well. Alternatively, a longer below-cut-off SIW section can also be implemented to increase isolation. Looking at the high-band it can be seen that the isolation is better than 40 dB which is due to the LPF in the WG for Port 2. If a higher isolation is required this LPF can be increased in order. However, this will lead to higher losses at 77 GHz. If a smaller isolation is required, the losses at 77 GHz can be minimized by reducing the order of the LPF.

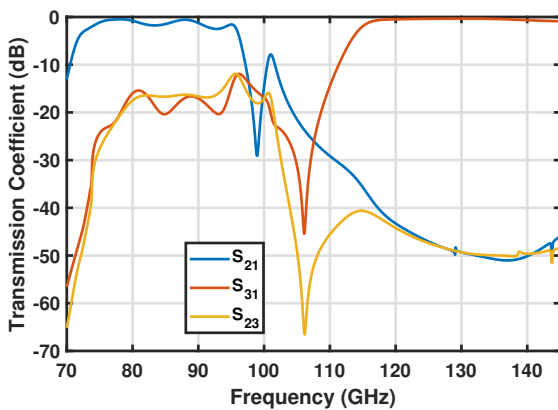


Fig. 5. Transmission coefficients of the single-ended transition.

Although losses are expected to be higher in the high-frequency WG, this is actually not the case. The higher losses in the low-frequency WG can be attributed to the filter. This can be visualized by plotting the losses as seen in Fig. 6. While the dielectric losses are higher at 130 GHz compared to 77 GHz, the aluminum losses are higher in the low-band. Due to additional bounces of the electromagnetic waves in this filter, there is more attenuation explaining the difference

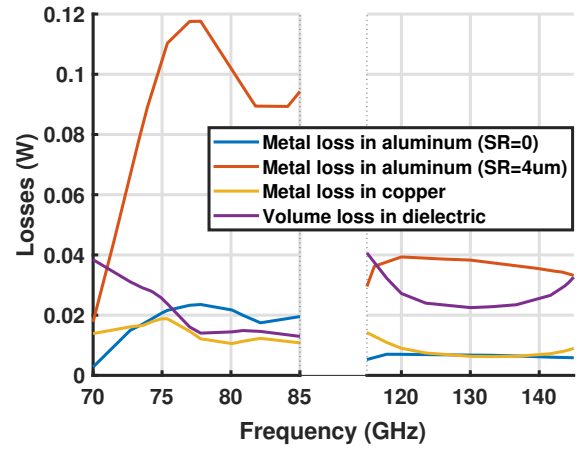


Fig. 6. Losses of the single-ended transition for an excitation of 0.5 W from Port 1.

with the 130 GHz WG. A plot of the metal loss in aluminum with a surface roughness of  $R_a = 4 \mu\text{m}$  in Fig. 6. A non-zero surface roughness makes even clearer the difference in losses between 77 GHz and 130 GHz and sketches a more realistic scenario for a manufactured prototype.

While these results only show simulated values, they are similar or performing better than the designs operating in between 70 GHz to 130 GHz reported in Table I. Additionally, these designs do not offer dual-band support. Nevertheless, some of the lower-frequency designs report better IL, mainly due to additional losses the diplexing part of this transition introduces.

#### IV. CONCLUSION

In this paper, a vertical SIW-to-metal WG transition is proposed, incorporating diplexing functionality. The dual-band SIW is able to diplex the RF signals in two distinct metal WGs operating at 77 GHz and 130 GHz. This design offers dual-band operation without sacrificing performance when using a single dual-frequency transition. Furthermore, it allows future automotive applications to aggregate data from two separate antenna systems working at 77 GHz and 130 GHz into a single IC. Moreover, the diplexer inside the transition is not as bulky as classical filter-based diplexers. This comes at the cost of a lower isolation.

The transition is able to achieve a 0.6 dB loss in the low-frequency band at 77 GHz while in the high-band at 130 GHz it achieves a 0.4 dB loss. The isolation is at least 15 dB at 77 GHz and at least 40 dB at 130 GHz. It should be mentioned that due to the fact that the manufacturing method is not yet decided, it is not known what additional losses will be introduced. However, a realistic surface roughness is simulated for the metal blocks to investigate their additional losses.

It is important to note that some of the losses in this design are due to the fact that the WGs taper outwards. This was done deliberately to ease future placement of external WG connectors for testing purposes. In a final implementation of

this transition this would not be necessary as the WGs will route to the antennas with the least possible length. Some remaining points for future research will be focused around the actual assembly and measuring of this design. Furthermore, a detailed analysis of the losses, highlighting what the actual transition loss is and what is caused by additional routing, would be an insightful addition to this work.

#### ACKNOWLEDGMENTS

This work is part of the research program Share-Waves with project number 19469, which is (partly) financed by the Dutch Research Council (NWO). Ivashina and Vilenskiy acknowledge the support of funding from the Sweden-Taiwan Collaborative Research Framework Project "Antenna Technologies for Beyond-5G Wireless Communication" from the Swedish Foundation for Strategic Research.

#### REFERENCES

- [1] Thrasher, B.A., "A 10 MHz to 80 GHz Low-Temperature Cofired Ceramic Ball Grid Array Board-to-Interposer Transition for Chip Scale Packages," no. 04, 2015. [Online]. Available: <https://doi.org/10.4416/JCST2015-00054>
- [2] A. R. Vilenskiy and Y. Zhang, "A Compact and Wideband MMIC to Ridge Gap Waveguide Contactless Transition for Phased Array Antenna Front-Ends," *IEEE Antennas and Wireless Propagation Letters*, pp. 1–5, 2023, conference Name: IEEE Antennas and Wireless Propagation Letters. [Online]. Available: <https://ieeexplore.ieee.org/abstract/document/10349922>
- [3] A. Hosseini-Fahrari, K. Mohammadpour-Aghdam, and R. Faraji-Dana, "Millimeter wave rectangular waveguide to grounded CPW transition on multi-layer substrate," in *2016 Fourth International Conference on Millimeter-Wave and Terahertz Technologies (MMWaTT)*, Dec. 2016, pp. 99–102, iSSN: 2157-0973. [Online]. Available: <https://ieeexplore.ieee.org/document/7869926>
- [4] A. U. Zaman, V. Vassilev, H. Zirath, and N. Rorsman, "Novel Low-Loss Millimeter-Wave Transition From Waveguide-to-Microstrip Line Suitable for MMIC Integration and Packaging," *IEEE Microwave and Wireless Components Letters*, vol. 27, no. 12, pp. 1098–1100, Dec. 2017, conference Name: IEEE Microwave and Wireless Components Letters. [Online]. Available: <https://ieeexplore.ieee.org/document/8100625>
- [5] A. Aljarosha, A. U. Zaman, and R. Maaskant, "A Wideband Contactless and Bondwire-Free MMIC to Waveguide Transition," *IEEE Microwave and Wireless Components Letters*, vol. 27, no. 5, pp. 437–439, May 2017, conference Name: IEEE Microwave and Wireless Components Letters. [Online]. Available: <https://ieeexplore.ieee.org/document/7911264>
- [6] D. Zhang, Z. Xu, Y. Xiao, and H. Sun, "A wideband siw-to-waveguide transition at w-band," in *2017 Sixth Asia-Pacific Conference on Antennas and Propagation (APCAP)*, Oct. 2017, pp. 1–3. [Online]. Available: <https://ieeexplore.ieee.org/document/8420609>
- [7] A. Roev, P. Taghikhani, R. Maaskant, C. Fager, and M. V. Ivashina, "A Wideband and Low-Loss Spatial Power Combining Module for mm-Wave High-Power Amplifiers," *IEEE Access*, vol. 8, pp. 194 858–194 867, 2020, conference Name: IEEE Access. [Online]. Available: <https://ieeexplore.ieee.org/abstract/document/9239291>
- [8] Y. Li and K.-M. Luk, "A Broadband V-Band Rectangular Waveguide to Substrate Integrated Waveguide Transition," *IEEE Microwave and Wireless Components Letters*, vol. 24, no. 9, pp. 590–592, Sep. 2014, conference Name: IEEE Microwave and Wireless Components Letters. [Online]. Available: <https://ieeexplore.ieee.org/document/6848864>
- [9] D. M. Pozar, *Microwave Engineering, 4th Edition | Wiley*. [Online]. Available: <https://www.wiley.com/en-us/Microwave+Engineering%2C+4th+Edition-p-9780470631553>
- [10] Y. Cassivi, L. Perregrini, P. Arcioni, M. Bressan, K. Wu, and G. Conciauro, "Dispersion characteristics of substrate integrated rectangular waveguide," *IEEE Microwave and Wireless Components Letters*, vol. 12, no. 9, pp. 333–335, Sep. 2002, conference Name: IEEE Microwave and Wireless Components Letters. [Online]. Available: <https://ieeexplore.ieee.org/document/1031925>

- [11] "Surface Roughness In 3D Printing." [Online]. Available: <https://xometry.pro/en-eu/articles/3d-printing-surface-roughness/>